Tutor/s

Dr. Juan Carlos Paniagua Valle
Departament de Química Física

Grau de Química

Treball Final de Grau

Theoretical study of the solvation effects on UV and IR spectra of the *N*-methylacetamide.

Estudi teòric dels efectes de la solvatació sobre l'espectre UV i IR de la *N*-metilacetamida.

Alejandro Martín Rodríguez

Juny de 2014

Universitat de Barcelona

Campus d'Excel·lència Internacional
BKC Barcelona Knowledge Campus

Els ordinadors són inútils. Només poden donar respostes.

Pablo Picasso

En primer lloc, voldria agrair al Dr. Juan Carlos Paniagua la seva constant dedicació a fer possible aquest treball que tanca la meva etapa com a estudiant de grau de química. Des del primer moment ha estat un plaer estar sota la teva molt valorada supervisió. Espero que en algun moment recuperis tot el temps que has dedicat a que això arribi a bon port i que els teus companys de departament et perdonin per arribar sistemàticament tard a l'hora de dinar cada dimecres.

D'una manera més indirecte però no menys important, voldria agrair a la facultat de química, concretament al professorat que en les seves classes ha permès que tingui una visió més global d'aquesta ciència (i art!) que és la química. Quedeu perdonats de les innumerables hores d'estudi que he hagut de dedicar en aquesta etapa. Han valgut la pena!

Als companys i companyes de trinxera amb els que he compartit moltes anècdotes i totes bones. Les xerrades a mig matí intentant no escaldar-nos la llengua amb el cafè extremadament calent del bar han estat un gran ajut per afrontar tota la feina que tocava fer, tot i que de vegades... Ens despistàvem. Només desitjo que continuem escaldant-nos la llengua junts!

Finalment, agrair a la família tot el recolzament incondicional que m'han donat al llarg de tots aquests anys, els ja passats i els que vindran.

Moltes gràcies a tots!

REPORT

CONTENTS

1. SUMMARY

This discussion examines the effects of solvation in ultraviolet and infrared spectra of *N*-methylacetamide at theoretical level. In the first part, the basis of DFT method is explained. In addition, a review of some basic concepts of spectroscopy and a short description of continuum solvation models and Grimme dispersion correction is made. In the second part, the effects of solvation are considered at three different levels: through a continuum description of solvation, using a solute-solvent cluster and using the same cluster embedded in an external continuum. To improve the overview on the effects of solvation on the IR and UV spectra, two types of continuum models are used: IEF-PCM (2003 and 2009 versions) and SMD. All calculations were carried out using two different basis sets: 6-31+G(d,p) and 6-311++G(d,p). In the latter, the dispersion correction proposed by Grimme was added.

Finally, it is analyzed and justified qualitatively the results of both spectra. For the IR spectra, the four fundamental bands amide I, II, III and NH stretching are studied. With respect to ultraviolet absorption, transitions $n \rightarrow \pi^*$ and $\pi \rightarrow \pi^*$ are studied.

Keywords: Time-dependent density functional theory, UV spectroscopy, solvation, IR spectroscopy, DFT, *N*-methyacetamide, computational chemistry.

2. RESUM

En aquesta discussió s'estudia l'efecte de solvatació en l'espectre infraroig i ultraviolat de la *N*-metilacetamida a nivell teòric. En una primera part s'expliquen les bases del mètode DFT. A més, es repassen alguns conceptes bàsics sobre espectroscòpia i es fa una petita introducció als models de solvatació continus i a una correcció de la dispersió proposada per Grimme. En la segona part, es considera l'efecte de la solvatació a tres nivells diferents: mitjançant una descripció continua de la solvatació, utilitzant un clúster solut-solvent i el mateix clúster en solvatació continua. Per tal de millorar la visió sobre l'efecte de la solvatació sobre els espectres IR i UV, s'han emprat dos tipus de models continus: IEF-PCM (versions de 2003 i 2009) i SMD. Tots els càlculs s'han dut a terme mitjançant dos conjunts de bases diferents: 6-31+G(d,p) i 6-311++G(d,p). En aquest últim, la correcció de la dispersió proposada per Grimme s'afegeix.

Finalment, s'analitzen i justifiquen de manera qualitativa els resultats obtinguts d'ambdós espectres. Per a l'espectre IR, s'estudien les quatre bandes fonamentals amida I, II, III i l'estirament NH. Respecte l'absorció a l'ultraviolat, les transicions $n \rightarrow \pi^*$ i $\pi \rightarrow \pi^*$ són estudiades.

Paraules clau: Time-dependent density functional theory, espectroscòpia UV, solvatació, espectroscòpia IR, DFT, *N*-metilacetamida, química computacional.

3. INTRODUCTION

In the last years, computational chemistry has become a paramount tool for theoretical chemists. This discipline uses several different methods to describe as far as possible the chemical system. Depending on the system and the objective of the calculation, it would be more useful a specific method than other just because of its way of approaching the real chemical system. The most popular quantum-mechanics-based methods for electronic structure calculations are Hartree-Fock (HF), Møller-Plesset perturbation theory (MPn) and semi-empirical methods among those focused on approximating the wave function of the system, and Kohn-Sham Density Functional Theory (KS-DFT) among those aiming at directly obtaining the electron density. All of them rely on the choice a basis set of functions to expand the molecular orbitals that will describe the electronic structure. There are plenty of different basis sets, most of them based Gaussian type orbitals (GTO), but also Slater type orbitals (STO) are used.

For huge molecules it is necessary to change the strategy because the computational time would be unviable for quantum methods, and then, molecular mechanics (classical mechanics) methods with its different force fields become the best option.

In this work, Density functional theory (DFT) will be used. The basis set used and other considerations would be explained along the document.

3.1. DENSITY FUNCTIONAL THEORY (DFT)

3.1.1. The philosophy

Most of the methods used to calculate different observables of the system of interest are based on the knowledge of its wave function. This is a tough work, since this function depends on one spin and three spatial coordinates for every electron in the system (assuming Born-Oppenheimer approximation, i.e. fixed nuclear positions). In terms of HF approximation, it is possible to express the state function as a Slater determinant of independent one-electron functions. This wave function can be dramatically improved in quality by removing this rough approach by including a dependence on interelectronic distances in the wave function (R12 methods). It all together seems like the issue is finely performed, but by using wave function

methods, in fact, there is a key disadvantage: The wave function is essentially uninterpretable. It is such a black box that answers accurately when questioned by quantum mechanical operators, but it offers little by way of sparking intuition.

When things start being complicated, it is a wise option to return to the essentials. For instance, why should it be working with a wave function? Can it be working with some physical observable in determining the energy (and other properties) of a molecule? By using what it is already known from quantum mechanics, the Hamiltonian depends on the positions and atomic numbers of the nuclei and the total number of electrons. This immediately suggest that the electron density ρ is a nice observable, because integrated all over the space yields the total number of electrons and it should be obvious that the nuclei positions corresponds to local maxima in the electron density. Though it all, it is one important issue left: The assignment of nuclear atomic numbers. It can be proved that the derivative of the spherically averaged density at the atomic position is proportional to the atomic number.

All the arguments above do not provide any formalism to construct the Hamiltonian operator, solve the Schrödinger's equation, and determine the wave functions and energies eigenvalues. Nevertheless, they suggest that some simplifications might be possible.

3.1.2. Rigorous foundation: Hohenberg-Kohn theorems

Early DFT models were provocative in its simplicity compared to wave-function-based approaches, but failed to describe properly molecular properties, yielding large errors and little impact on chemistry. Even though, the method succeeded in solid-state physics (where the enormous system size puts a premium on simplicity).

One of the simplest models was the uniform electron gas, also known as "jellium". This system is composed of an infinite number of electrons moving in an infinite volume characterized by a uniformly distributed positive charge. This model breaks down for molecules since it ignores the energetic effects associated with correlation and exchange in the calculation of interelectronic repulsion. As result, all molecules are unstable relative to dissociation into their constituent atoms.

In 1964, the theory was finally rigorously founded. Hohenberg and Kohn proved two key theorems to establish a variational principle for DFT calculations and then, legitimate the method as a quantum mechanical methodology.

3.1.2.1. The Hohenberg-Kohn existence theorem

The first theorem states the ground-state density determines the external potential. This potential defines the interaction between electrons and nuclei.

The proof of the existence theorem proceeds via *reductio ad absurdum:* Let us assume that two different external potentials can be obtained from the same non-degenerated ground-state density ρ_0. This two potentials, v_a and v_b and its different Hamiltonians in which they appear H_a and H_b will be associated to a ground-stated wave function ψ_0 and its associated eigenvalue E_0.

From the variational theorem of molecular orbital theory its known that

$$E_{0,a} < \langle \psi_{0,b} \mid H_a \mid \psi_{0,b} \rangle \tag{3.1}$$

And can be rewrite as

$$\begin{aligned} E_{0,a} &< \langle \psi_{0,b} \mid H_a - H_b + H_b \mid \psi_{0,b} \rangle \\ E_{0,a} &< \langle \psi_{0,b} \mid H_a - H_b \mid \psi_{0,b} \rangle + \langle \psi_{0,b} \mid H_b \mid \psi_{0,b} \rangle \\ E_{0,a} &< \langle \psi_{0,b} \mid H_a - H_b \mid \psi_{0,b} \rangle + E_{0,b} \end{aligned} \tag{3.2}$$

Since the potentials v are one-electron operators, the integral in the last line can be expressed in terms of the ground-state density

$$E_{0,a} < \int [\upsilon_a(r) - \upsilon_b(r)]\rho_0(r)dr + E_{0,b} \tag{3.3}$$

$$E_{0,b} < \int [\upsilon_b(r) - \upsilon_a(r)]\rho_0(r)dr + E_{0.a} \tag{3.4}$$

As there is no distinction made between a and b, it is possible to switch the indices in Eq. (3.3) to obtain Eq. (3.4). Now, adding inequalities

$$\begin{aligned} E_{0,a} + E_{0,b} &< \int [\upsilon_a(r) - \upsilon_b(r)]\rho_0(r)dr + \int [\upsilon_a(r) - \upsilon_b(r)]\rho_0(r)dr \\ &\quad + E_{0,b} + E_{0,a} \\ E_{0,a} + E_{0,b} &< \int [\upsilon_a(r) - \upsilon_a(r) - \upsilon_b(r) + \upsilon_b(r)]\rho_0(r)dr + E_{0,b} + E_{0,a} \\ E_{0,a} + E_{0,b} &< E_{0,b} + E_{0,a} \end{aligned} \tag{3.5}$$

The expression achieved left an impossible result, which must indicate that the initial assumption is incorrect. So, a non-degenerated ground-state density must determine the external potential, thus, the Hamiltonian and finally, the wave-function.

Note moreover that the Hamiltonian determines also all excited-state wave-functions as well. But. Is it possible to calculate any excited state? Gunnanrsson and Lundqvist, using group

theory, proved that only the lowest energy (non-degenerated) state within each irreducible representation of the molecular point group can be calculated. That means, for instance, the densities of the singlet A_g and triplet B_{1u} states of *p*-benzyne are well defined, but nothing can be said about triplet A' state of *N*-protonated 2,5-didehydropyridine, since there is a lower energy singlet A'. The development of DFT formalism to handle arbitrary excited states remains a subject of active research.

3.1.2.2. The Hohenberg-Kohn variational theorem

The first theorem is an existence theorem, but gives no information about how to predict the density of a system. Hohenberg and Kohn showed in a second theorem that, as with MO theory, the density obeys a variational principle.

Let us assume a well-behaved candidate density that determines ψ_{cand} and its Hamiltonian. Invocating the variational theorem

$$\langle \psi_{cand} \mid H_{cand} \mid \psi_{cand} \rangle = E_{cand} \geq E_0 \tag{3.6}$$

So, in principle, it is possible to keep choosing different densities and those that provide lower energies, are closer to correct. But first, there is no formalism to improve the candidate densities rationally, and second, it is not avoided to solve Schrödinger equation - It is well known to do that. Nevertheless, most of practical implementations requires to calculate a wave-function for a simpler hypothetical system.

Such an approach to reach an optimal density was propose in 1965 through a self-consistent field procedure by Kohn and Sham. This SCF will be discussed in section 3.1.4.

3.1.3. Improving the Hohenberg-Kohn theorems: Levy theorems

In 1979, M. Levy demonstrated Hohenberg and Kohn theorems by using a formulation based on restricted minimizations. This new formulation expands the original theorems and connects them closely with the variational theorem.

3.1.3.1. Improving the Hohenberg-Kohn variational theorem

For a n-electronic molecule, it is possible to express the Hamiltonian as

$$\hat{H} = \sum_{i=1}^{n} -\frac{\nabla_i}{2} + \sum_{i=1}^{n-1}\sum_{j>i}^{n} \frac{1}{r_{ij}} + \sum_{i=1}^{n}\sum_{A=1}^{N} -\frac{Z_A}{r_{iA}} \tag{3.7}$$

Where the first term is the kinetic energy operator (T_{el}), the second is the interelectronic repulsion operator (V_{el}) and the last term is the attractive potential between the electrons and the nuclei($V_{nuc\text{-}el}$).

The monoelectronic density of a wave-function ψ and the wave-function itself is related through the defined integral

$$\rho(\vec{r}) = n\int_{\omega_1}\int_{\vec{r}_2}\int_{\omega_2}\cdots\int_{\vec{r}_n}\int_{\omega_n} |\psi(\vec{r},\omega_1,\vec{r}_2,\omega_2,...,\vec{r}_n,\omega_n)|^2 \times d\vec{r}, d\omega_1, d\vec{r}_2, d\omega_2,..., d\vec{r}_n, d\omega_n \tag{3.8}$$

Eq. (3.8) shows that different wave-functions could yield to the same density. This permits to express the variational theorem (Eq. (3.6)) as a two-steps minimization:

1. For a target density, the wave-functions ψ_ρ with that density and energy minimized are chosen.
2. From the set generated before, the minimal energy function is chosen.

After all, the process can be expressed as

$$E_0 = \min_{\rho}\left(\min_{\psi_\rho}\left\langle \psi_\rho \mid \hat{H}\psi_\rho \right\rangle\right) = E[\rho_0] \tag{3.9}$$

Thus, the connection with the variational theorem is already shown. If it were possible to know the explicit form of $E[\rho]$, it would be possible to minimize directly the functional, and hence, there would be no need of calculating ψ_ρ.

Yet another highlight: If it combines Eq. (3.7) and Eq. (3.9)

$$E[\rho] = \left\langle \psi_\rho^{\min} \mid \left(\hat{T}_{el} + V_{el}\right)\psi_\rho^{\min} \right\rangle + \left\langle \psi_\rho^{\min} \mid V_{nuc-el}\psi_\rho^{\min} \right\rangle \tag{3.10}$$

As the former term uniquely depends on the number of electrons, it is the same functional for every system with the same number of electrons. So, it can be redefined as the universal functional $F[\rho]$.

$$F[\rho] = \left\langle \psi_\rho^{\min} \mid \left(\hat{T}_{el} + V_{el}\right)\psi_\rho^{\min} \right\rangle \tag{3.11}$$

The minimization of this functional is perfectly equivalent as minimizing Eq. (3.9) as the latter term of Eq. (3.10) yields to the same value for different wave-functions with the same density. If the universal functional were perfectly known, the sum of the latter term to the former would be enough to obtain the functional $E[\rho]$.

$$E_0 = F[\rho] + V_{nuc-el} \tag{3.12}$$

Thus, Levy proved and improved the Hohenberg-Kohn variational theorem. The original theorem was restricted to non-degenerated ground-state. This new formulation expands the theory to degenerated ground-states.

Hohenberg-Kohn and Levy formulation explain that if the wave-function is known, the density is also known, but not *vice versa*. As it is able only to know a wave-function that has the same density, the properties do not have to be the expected ones. This would be a big limitation, but actually it is not a big issue since the energy is determined by Eq. (3.12) and the other properties can be easily related with the density.

3.1.3.2. Improving the Hohenberg-Kohn existence theorem

As in the original enunciation, this theorem proves that the external potential is uniquely defined given a monoelectronic density. In Levy's formulation, the Hohenberg-Kohn theorem is expanded to degenerated ground-states: any degenerated density of the ground-state yields to the same external potential. The external potential is defined by

$$v_{ne}(\vec{r}) = \left(-\frac{\delta F[\rho]}{\delta \rho(\vec{r})} \right)_{\rho=\rho_0} \tag{3.13}$$

An intuitive justification of this expression: If the monoelectronic density of the ground-state (or any excited state) is known, is possible to calculate the number of electrons, which determinates the operators T_{el} and V_{el}. The positions of the nuclei are defined where the density has a peak, which slope is dependent of the charge of the nuclei. Hence, it is possible to calculate the operator $V_{nuc\text{-}el}$.

Using the definition of functional derivative, it is possible to prove Eq. (3.13)

$$\left(\frac{\partial F[\rho_0 + \varepsilon g(\vec{r})]}{\partial \varepsilon} \right)_{\varepsilon=0} = \int_{\Re^3} \left(\frac{\delta F[\rho]}{\delta \rho(\vec{r})} \right)_{\rho=\rho_0} g(\vec{r}) d\vec{r} \tag{3.14}$$

where ε is a real parameter and $g(r)$ is an arbitrary function of r. For proving Eq. (3.13), ρ is defined as

$$\rho = \rho_0 + \varepsilon g(\vec{r}) \tag{3.15}$$

where g is any function that accomplishes the normalization of ρ, that is

$$\int_{\Re^3} g(\vec{r}) d\vec{r} = 0 \tag{3.16}$$

Combining Eq. (3.16), Eq. (3.12) and Eq. (3.9).

$$E_0 = \min_{\rho} E[\rho] = \min_{\varepsilon}\{F[\rho_0 + \varepsilon g(\vec{r})] + V_{nuc-el}[\rho_0 + \varepsilon g(\vec{r})]\}$$
$$= \min_{\varepsilon}\left\{F[\rho_0 + \varepsilon g(\vec{r})] + \int_{\Re^3} v_{ne}(\vec{r})[\rho_0 + \varepsilon g(\vec{r})]d\vec{r}\right\} \quad (3.17)$$

As ρ_0 is the minima of *E[ρ]* (first theorem), ε must equal 0. Also, ε=0 must be a stationary point

$$\left(\frac{\partial\left\{F[\rho_0 + \varepsilon g(\vec{r})] + \int_{\Re^3} v_{ne}(\vec{r})[\rho_0 + \varepsilon g(\vec{r})]d\vec{r}\right\}}{\partial\varepsilon}\right)_{\varepsilon=0} = 0 \quad (3.18)$$

Hence, using Eq. (3.14)

$$\int_{\Re^3}\left\{\left(\frac{\delta F[\rho]}{\delta\rho(\vec{r})}\right)_{\rho=\rho_0} + v_{ne}(\vec{r})\right\} g(\vec{r})d\vec{r} = 0 \quad (3.19)$$

Eq. (3.19) shows that for any *g(r)* function, the term in braces must be constant.

$$\left(\frac{\delta F[\rho]}{\delta\rho(\vec{r})}\right)_{\rho=\rho_0} + v_{ne}(\vec{r}) = c \quad (3.20)$$

Allowing this constant to be zero, Eq. (3.13) is achieved.

3.1.4. The Kohn-Sham self-consistent field methodology

The main blockage to develop a DFT method is the lack of awareness of the universal functional. W. Kohn and L. J. Sham propose in 1965 a strategy to approach the external potential. They used a hypothetic n-electron independent system under a multiplicative external potential $v^{KS}(r)$ with an associated ground-state monoelectronic density ρ_0^{KS} equal to the density of the real system.

This strategy works under the Kohn-Sham conjecture: If the Kohn-Sham system exist, then, the density of the real system is representable. If just one Kohn-Sham system is enough to perform the target density of the real system, that system is called pure-state representable. If a weighted sum of monoelectronic densities is needed to perform the real system, then the system is *Ensemble representable*.

The Hamiltonian of a Kohn-Sham system is defined as

$$\hat{H}^{KS} = \hat{T}_{el} + \hat{V}_{ne}^{KS} = \sum_{i=1}^{n}\left(\frac{-\nabla}{2} + v_{ne}^{KS}(\vec{r}_i)\right) = \sum_{i=1}^{n}\hat{h}^{KS}(\vec{r}_i) \quad (3.21)$$

where the operator V_{el} does not appear as long as the electrons have no interaction between them and h^{KS} is the monoelectronic Kohn-Sham operator.

As in the Hartree-Fock method, the separability of H^{KS} allows to express the ground-state wave-function as a Slater determinant built up with n eigenspinorbitals of the KS operator with lower energy.

$$\Phi^{KS} = \frac{1}{\sqrt{n!}}\left|\psi_1^{KS}(\omega_1)...\psi_n^{KS}(\omega_n)\right| \tag{3.22}$$

with

$$\hat{h}^{KS}(\vec{r}_i)\psi_i^{KS}(\vec{\omega}) = \varepsilon_i^{KS}\psi_i^{KS}(\vec{\omega}) \tag{3.23}$$

and energy

$$E^{KS} = \sum_{i=1}^{n}\varepsilon_i^{KS} \tag{3.24}$$

If the Kohn-Sham system ground-state is degenerated, there is no problem as long as all Slater determinants have the same electronic densities (i.e. non-degenerated states or one unpaired electron in a non-degenerated orbital). But if the Kohn-Sham system has, for instance, a $1s^2 2s^2 2p_x^2$ configuration, this would have the same energy as a $1s^2 2s^2 2p_x^1 2p_y^1$ system (both are degenerated), but not the same density. Hence, it cannot be know which density corresponds to the real system. Although several strategies are studied to approach this cases, it will be focused on the non-degenerated cases and those with one despaired electron in a non-degenerated orbital.

Both theorems apply to any n-electronic system; thus, we can apply them to a Kohn-Sham system. The universal functional *F[ρ]* to be minimized then reduces to

$$F^{KS}[\rho] = T^{KS}[\rho] = \left\langle \Phi_\rho^{\min} \mid \hat{T}_{el}\Phi_\rho^{\min} \right\rangle \tag{3.25}$$

where the wave-function that minimize the functional can be expressed as a Slater determinant. The previous equation leads to the modification of Eq. (3.13)

$$v^{KS}(\vec{r}) = -\left(\frac{\delta T^{KS}[\rho]}{\delta\rho(\vec{r})}\right)_{\rho=\rho_0} \tag{3.26}$$

Now it is time to impose ρ_0 to be the density of the real system. Nevertheless, the wave-function that minimizes *F[ρ]* is not the same that minimizes $F^{KS}[\rho]$. An attempt to do so, is to

adopt $T^{KS}[\rho]$ as an approach to $T[\rho]$ and the classical columbic repulsion $J[\rho]$ as an approach to $V_{el}[\rho]$

$$J[\rho]=\frac{1}{2}\int_{\vec{r}_1}\int_{\vec{r}_2}\frac{\rho(\vec{r}_1)\rho(\vec{r}_2)}{r_{12}}d\vec{r}_1 d\vec{r}_2 \tag{3.27}$$

where the 1/2 factor is included so as not double count every pair of electrons. To take into account the error produced in such approximation, a new functional known as exchange-correlation functional $E_{xc}[\rho]$ is introduced.

$$E_{xc}[\rho]=T[\rho]-T^{KS}[\rho]+V_{el}[\rho]-J[\rho] \tag{3.28}$$

This new functional is also universal as long as all the terms appearing in its definition are universal. The E_{xc} functional has to gather the following considerations even though both approximations are fair enough and the functional is small:

The lack of electronic correlation in the Slater determinant used for calculating $T^{KS}[\rho]$.

- The lack of electronic correlation in $J[\rho]$ calculation.
- Exchange effects
- The self-repulsion introduced by the use of $J[\rho]$.

The exchange effects are, by far, the largest of them all. Through an analogous deduction used for Eq. (3.13), the correlation-exchange potential is define as

$$v_{xc}(\vec{r})=\left(\frac{\delta E_{xc}[\rho]}{\delta\rho(\vec{r})}\right)_{\rho=\rho_0} \tag{3.29}$$

and then, combining Eq. (3.29), Eq. (3.13) and Eq. (3.26)

$$v^{KS}(\vec{r}_1)=v_{ne}(\vec{r}_1)+\int_{\vec{r}_2}\frac{\rho_0(\vec{r}_2)}{r_{12}}d\vec{r}_2+v_{xc}(\vec{r}_1) \tag{3.30}$$

Sadly, the real monoelectronic density is still unknown. But now (and assuming an approach to v_{xc}), a self-consistent field calculation is used to determine v^{KS} (figure 3.1).

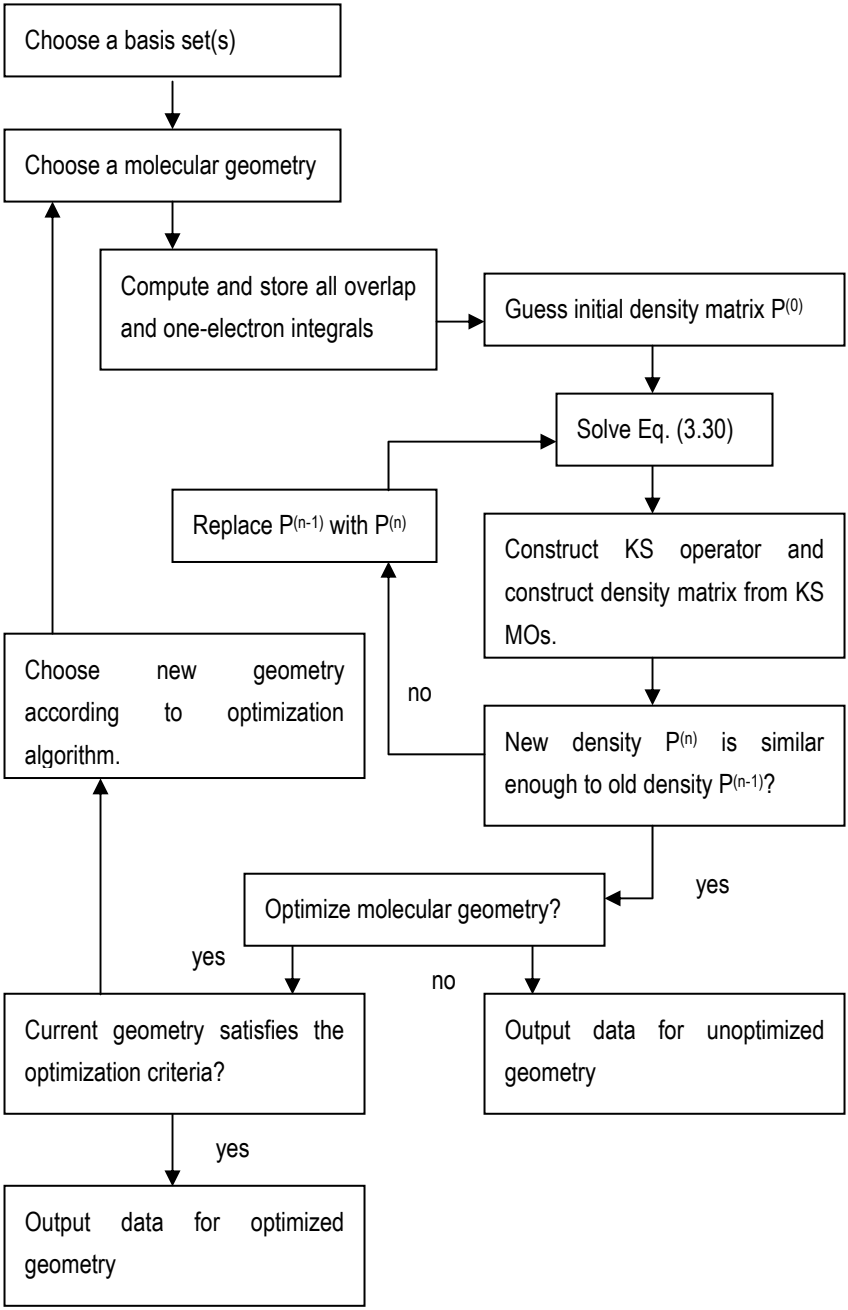

Figure 3.1. Kohn-Sham Self-consistent field

Several approaches to v_{xc} are briefly explained in the next headland.

The density from the KS occupied orbitals is calculated through

$$\rho_0 = \sum_{i=1}^{oc} n_i \, | \psi_i (\vec{r}) |^2 \tag{3.31}$$

where n_i is the occupation number of the orbital *i*. With Eq. (3.31) it is possible to build up a gridbox with a defined density for a given point of space.

3.1.4.1. Exchange-correlation functionals

In this subsection it will be enumerated some exchange-correlation functionals to use in the previous SCF. In many of this functionals empirical parameters appear.

Usually, the functional dependence of E_{xc} is expressed as an integral of the electron density times an energy density ε_{xc}. The E_{xc} is obtained with

$$E_{xc}[\rho(r)] = \int \rho(r) \varepsilon_{xc}[\rho(r)] dr \tag{3.32}$$

Another convention expresses the electron density in terms of an effective radius such that exactly one electron would be contained within the sphere defined by that radius were it to have the same density throughout as in its centre

$$r_S(r) = \left(\frac{3}{4\pi\rho(r)} \right)^{1/3} \tag{3.33}$$

For open shell systems the spin density at any position is typically expressed in terms of ζ, the normalized spin polarization

$$\zeta(r) = \frac{\rho^{\alpha}(r) - \rho^{\beta}(r)}{\rho(r)} \tag{3.34}$$

This considerations lead to what is known as “pure” functionals:

- *Local density approximation (LDA*): The value of ε_{xc} at some position r can be computed exclusively from the value of ρ and is single-valued at every position.
- *Local spin density approximation (LSDA)*: LDA is extended to a spin-polarized formalism.
- *Generalized gradient approximation (GGA)*: One obvious way to improve the correlation functional is to make it depend not only on the local value of the

density, but on the extent to which the density is locally changing. So, LDA is gradient corrected.

- *meta-GGA (m-GGA)*: The second derivative is added to GGA.

There are other types of pure functionals, but the previous types are the most representative.

Another class is that of the so-called hybrid functionals, which mix pure functionals with the Hartree-Fock exchange energy to improve the results of both individual methods. One of the most popular within this class, the B3LYP functional is used in the calculations of this work and corresponds to

$$E_{xc}^{B3LYP} = (1-a)E_x^{LSDA} + aE_x^{HF} + b\Delta E_x^B + (1-c)E_c^{LSDA} + cE_c^{LYCP} \quad (3.35)$$

where a, b and c take the values 0.20, 0.72 and 0.81.

3.2. UV AND IR SPECTRA

In this section it will be provided some qualitative basis of absorption spectroscopy, specially for ultra-violet (UV) and infrared (IR) wavelengths, needed to understand the results of the present work. Perhaps this part is not worth it for an specialist reader, but it may be a good reminder for this topic.

3.2.1. The electromagnetic radiation

A classical view of the electromagnetic radiation is to consider that it is produced when charged particles are accelerated by forces acting on them. This perturbation propagates through the space carrying radiant energy at speed of light in vacuum. As an electromagnetic wave, it has both electric (*E*) and magnetic (*B*) oscillating fields perpendicular to each other and also to the direction of propagation (*k*). James Clerk Maxwell demonstrate through his equations that electricity, magnetism and light are because of the same phenomena: the electromagnetic field.

The *λ* shown in figure (3.2) is called *wavelength*, the length between two points of the same phase. Through this magnitude, the electromagnetic waves can be classified. This classification is known as *electromagnetic spectrum* (figure 3.3).

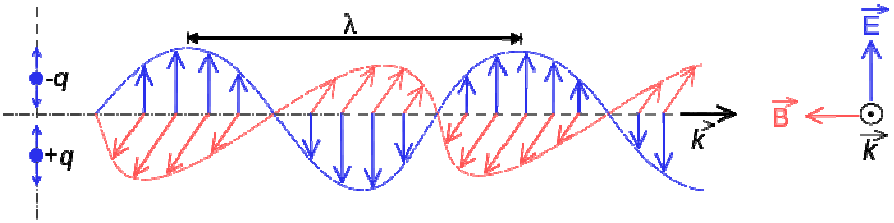

Figure 3.2. Electromagnetic wave.

(Emmanuel Boutet, 03/06/14 via Wikimedia commons, Creative commons attribution)

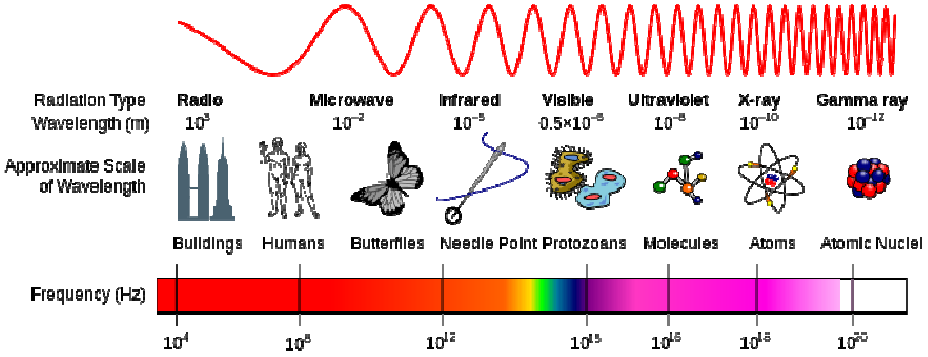

Figure 3.3. Electromagnetic spectrum.

(Inductiveload, 03/06/14 via Wikimedia commons, Creative commons attribution)

3.2.2. Historical background: The need of the quantum physics

As an electromagnetic waves carry energy, this energy can be absorbed or emitted by a molecule (and by extension, a macroscopic body). In late s.XIX, the emission spectra of an incandescent body was an object of study. The Stefan-Boltzmann law predicted the total intensity of radiation given a temperature, and the Wien Law predicted, given a temperature, which wavelength was the most emitted.

All seemed well until Rayleigh and Jeans predicted that, for classical physics, a body with a non-zero temperature should emit ultra-violet radiation. Even X rays and gamma rays. In fact, the human body at 37ºC would shine in the darkness! This unbelievable (but true at classical physics level) prediction is known *as Rayleigh-Jeans Catastrophe or Ultra-violet catastrophe*.

Luckily, in 1900, the German physicist Max Planck achieved the solution to the ultra-violet catastrophe: the energy exchange between the electromagnetic wave and the matter should be

quantized. The Planck law performs correctly the radiation emitted by an incandescent body. The main idea was that the energy can only be exchanged with the matter in packs of energy defined by

$$E = h\upsilon \tag{3.36}$$

where *h* is the Planck constant and has a value of $6{,}626 \cdot 10^{-34}$ J·s and *v* is the frequency of the wave or oscillation. This simple equation represents the birth of quantum physics.

In 1905, Albert Einstein extended Planck's hypothesis to explain the photoelectric effect.

From Planck and Einstein works, Louis De Broglie developed the *wave-particle duality*. This theory proposes that elementary particles are not only particles, but also waves. The elemental particle associated to the electromagnetic waves of light are *photons*. The energy of a photon of a given wavelength is defined by Eq. (3.36).

So, actually, the interpretation of an absorption can be approximated to the collision of a photon and the molecule and/or an electron. In this collision, the energy is exchanged and the system suffers an electronic change (usually in the visible or UV range) or a vibrational change (in the IR range).

3.2.3. The IR and UV-visible absorption spectra

In fact, a molecule can absorb a wide range of the electromagnetic spectra, but only in some specific wavelengths. This quantized wavelengths are determined by the characteristics of the molecule.

The changes in the vibrational energy of the molecule produce absorption bands in the IR range, from the visible limit to about 100 μm.

A molecule can vibrate in many ways and each way of vibrating is called *vibration mode*. The number of vibration modes for linear molecules (for instance CO_2) is 3N-5, where N is the number of atoms. A non-linear molecule has 3N-6 different vibrations. The classical vibrations that can be seen in a -CH_2- group and other groups are shown in Figure 3.4.

Nevertheless, there are some special effects: in some cases, overtone bands are shown. This bands are because of the absorption of a photon that leads to a double excited vibrational state (i.e. the vibrational state goes from fundamental state to the second excited state). Such bands appear at twice the energy of the fundamental. Furthermore, second or third overtones could be seen, but the intensity of those bands is smaller.

Also, the so-called *combination modes* involves more than one normal mode. This phenomenon arises when the energy of the bands implied are similar in energy.

The UV-visible range of absorption produces a change in the electronic configuration of a molecule. When an electron is excited by a photon, this electron gain energy enough to promote to a higher energy orbital. In fact, a given electron will only interact with a photon that has the exact energy between the fundamental electronic state of the molecule and n the excited state. Where n is the first, second and so excited states. Actually, same idea is perfectly applicable to the IR spectra and other absorption spectra.

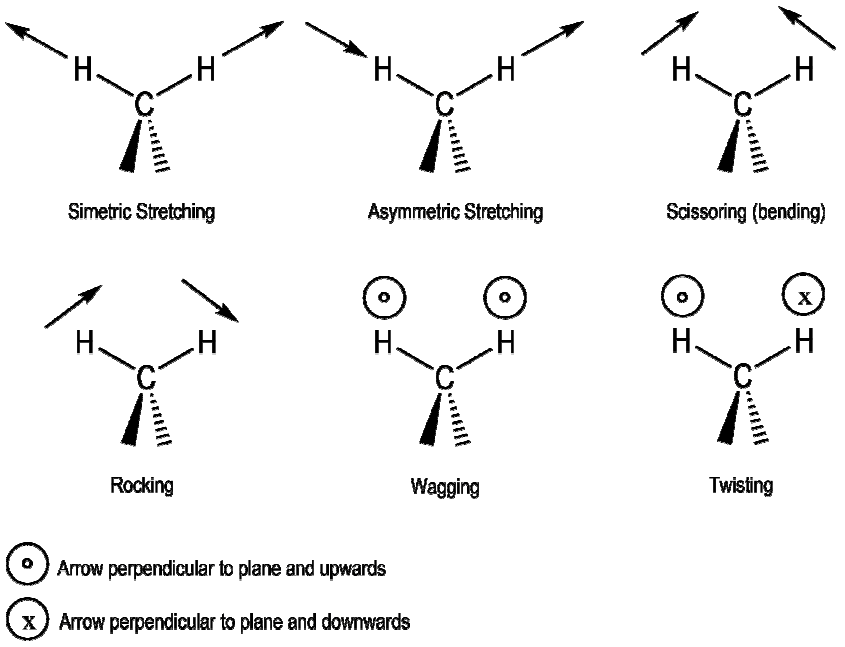

Figure 3.4. Classical vibrations of a -CH_2- group. In a complex molecule a mix of them can be seen.

The energy of that photon can be approached as the energy difference between the orbital where the electron actually is and the orbital to which the electron will be promoted. In spite of this approximation, another fact must be considered: when an electron is promoted, the whole repulsion between electrons is affected. Thus, it is necessary to take into account the variation of the repulsion once the promotion is completed. This concept yields to excitation energies around the energy difference between the orbitals implied, but can be greater or lower than the

approached. On the other hand, molecular geometry can change upon an electronic transition. If this is not taken into account, the energy calculated is the so-called *vertical transition excitation energy*. After all, even if a photon has the fine energy to promote either an electron or a vibrational mode, the transition must accomplish what is known as *selection rules*. The more rules a transition satisfy, the greater the intensity of that transition will be.

For an electronic transition:

- The transition must be allowed by electric dipole
- The transition must be allowed by magnetic dipole
- The transition must keep the spin of the system

For a vibrational transition only apply the dipole moment rules as the spin is kept the same for granted.

To summarise this section, it was explained what the radiation is, how the radiation interacts with matter and what requirements are needed to make this happen. Nevertheless, a very important final issue left: if the energy of an photon must be exactly the difference between states either in vibrational or electronic transitions, why a band is shown when an spectrum is performed?

Figure 3.5 illustrates the *Frank-Condon principle*. This principle says that a transition is more probable if there is no change in the atomic positions. The electronic transitions are essentially instantaneous in comparison to the movement of the nuclei. Hence, if a molecule promotes an electron to a new electronic level, the new vibrational level must have a compatible geometry with the previous one. The blue line shows a vertical transition from the fundamental electronic state (E_0) and fundamental vibrational state (v=0) to the first electronic state (E_1) and second excited vibrational state (v=2). So, under Franck-Condon principle, an electronic excitation will carry an intrinsic change on the vibrational level, either to a greater or a lower level. Adding that given a temperature, a molecule will occupy a certain distribution of the firsts vibrational levels (if the energetic difference between levels is low), it is possible to understand why, although the energy is quantized, not a line but a band is shown when a UV-visible spectrum is performed.

As an electronic state has some vibrational levels associated, a vibrational level has some rotational levels associated. An analogous idea can be used to understand why a IR-spectrum produce bands: Given a temperature, a molecule will occupy different rotational levels in a

certain distribution so, for just one excitation, a band will be shown. Once rotational excitations are reached, quantum nature can be seen: a pure rotational spectrum shows, finally, lines.

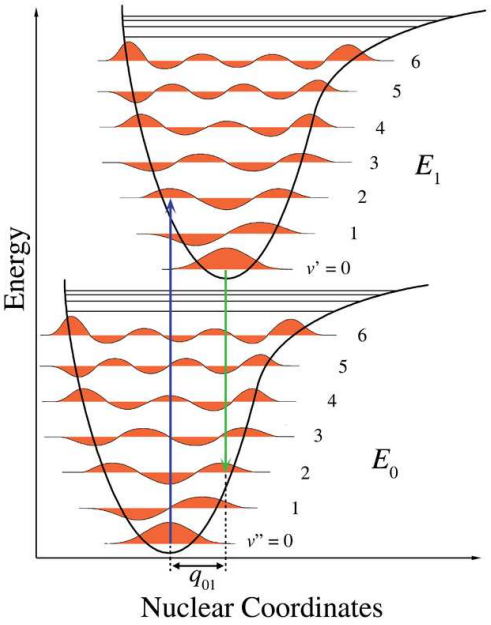

Figure 3.5. A Franck-Condon diagram.

(Mark M. Somoza, 04/06/13 *via Wikimedia commons, Creative commons attribution)*

3.2.4. Time-Dependent DFT (TD-DFT)

Now, it is time to focus on how to compute an electronic absorption spectrum. An intuitive way of deal with this issue is to calculate the ground-state energy and the target excited state energy and then, calculate the energy difference. This method actually works, but it is impossible to handle if the objective is to study the whole spectrum. Furthermore, it was already shown in section 3.1.4 that DFT can only know for sure the energy of the lowest non-degenerated excited state of an specific irreducible representation. Hence, only a few bands could be performed with DFT.

A first approximation to calculate the excitation energies is to use the differences between the ground-state Kohn-Sham eigenvalues. The Kohn-Sham orbitalic energies have no direct physical meaning (with the exception of the highest occupied one), but sometimes are used to interpret experimental observations.

More elaborated approaches are

- To restrict the variational principle to wave-functions of an specific symmetry.
- The so-called *generalized adiabatic connection Kohn-Sham formalism*, where each state of the many-body system is adiabatically connected to a Kohn-Sham state.
- Searching for local extreme of the ground-state energy functional.
- Calculating multiple energies by a Hartree-Fock-Slater method.
- *Ensemble DFT*, where energy is obtained through an ensemble of the ground state with some excited states.

Alternatively, the excitation energies can be obtained by knowing how the system responds to a small time-dependent perturbation, and can therefore be readily extracted from a TD-DFT calculation. The Time-dependent DFT theory is an extension of DFT to deal with time-dependent systems. This theory stands in virtue of the *Runge-Gross theorems*. These theorems are completely analogous to H-K/Levy theorems but, this time, the density functionals (and the density itself) are time dependent.

Within TD-DFT, two different regimes can be distinguished:

1. For a strong external potential, a full solution of the TD-DFT Kohn-Sham equations (Eq. (3.23) and Eq. (3.31)) is needed.
2. If the external time-dependent potential is small, the solution of the Kohn-Sham equations can be avoided and the *linear response theory* can be used.

The former assumption is necessary for intense laser fields (good to remember that the external field can also hold this kind of external interactions). The latter will be used to derivate a self-consisted field to achieve the excitation energies of a target system. Here is presented a simplified derivation of the SCF. A more extended derivation of Runge-Gross theorems, the exchange-correlation TD-functionals (analogous to TD-functionals) and the whole methodology can be consulted in ref. 5 and 6.

So, a change on the density when the system is perturbed by a small change of the external potential is described by

$$\delta n_{\sigma}(r,\omega) = \sum_{\sigma'} \int dr' \, \chi_{\sigma\sigma'}(r,r',\omega)\delta \upsilon_{ext\sigma'}(r',\omega) \tag{3.37}$$

where χ function is the so-called *linear density response function*, $\delta v_{ext\sigma'}$ is the perturbation on the system. This equation is good enough to evaluate χ for a linear excitation spectrum, but it is easily extended to study nonlinear responses or cases where the external field is not a small perturbation.

Following a similar strategy used to elaborate a SCF, Eq. (3.37) can be used for a Kohn-Sham system. In terms of the unperturbed stationary Kohn-Sham orbitals, it reads:

$$\chi^{KS}_{\sigma\sigma'}(r,r',\omega)=\delta_{\sigma\sigma'}\sum_{jk}^{\infty}(f_{k\sigma}-f_{j\sigma})\frac{\psi_{j\sigma}(r)\psi^{*}_{j\sigma}(r')\psi_{k\sigma}(r')\psi^{*}_{k\sigma}(r)}{\omega-(\varepsilon_{j\sigma}-\varepsilon_{k\sigma})+i\eta} \tag{3.38}$$

where ψ and ε are Kohn-Sham orbitals and its eigenvalues, f is the occupation number of the *jth/ith* orbital and η is a positive infinitesimal. Using Eq. (3.30) adapted to time dependence we can obtain the linear change of the Kohn-Sham potential

$$\delta\upsilon^{KS}_{\sigma}(r,\omega)=\delta\upsilon_{ext\sigma}(r,\omega)+\int dr'\frac{\delta n(r',\omega)}{|r-r'|}+\sum_{\sigma'}\int dr'\,f_{xc\sigma\sigma'}(r,r',\omega)\delta n(r',\omega) \tag{3.39}$$

The Fourier transform of the xc functional has been introduced

$$f_{xc\sigma\sigma'}[n_{\uparrow},n_{\downarrow}](r,r',t-t')=\frac{\delta\upsilon_{xc\sigma}[n_{\uparrow},n_{\downarrow}](r,t)}{\delta n_{\sigma'}(r',t')} \tag{3.40}$$

Combining Eq. (3.37) for a Kohn-Sham system and Eq. (3.39)

$$\delta n_{\sigma}(r,\omega)=\sum_{\tau}\int dr'\chi^{KS}_{\sigma\tau}(r,r',\omega)\left[\delta\upsilon_{ext\tau}(r',\omega)+\int dx\frac{\delta n(x,\omega)}{|r'-x|}+\right.$$
$$\left.+\sum_{\tau'}\int dx f_{xc\tau\tau'}(r',x,\omega)\delta n(x,\omega)\right] \tag{3.41}$$

As the Kohn-Sham system and the real system must have the same change on the density, combining time again Eq. (3.30), but this time for the real system

$$\chi_{\sigma\sigma'}(r,r',\omega)=\chi^{KS}_{\sigma\sigma'}(r,r',\omega)+\sum_{\tau\tau'}\int dx\int dx'\,\chi_{\sigma\tau}(r,x,\omega)\times$$
$$\times\left[\frac{1}{|x-x'|}+f_{xc\tau\tau'}(x,x',\omega)\right]\chi^{KS}_{\tau'\sigma'}(x',r',\omega) \tag{3.42}$$

Eq. (3.42) is a formally exact representation of the density of the interacting system. Nevertheless, the f_{xc} functional is not known and an approximation must be used. Different

approaches are available. The functionals seen in section 3.1.4.1 have their time-dependent relatives and also other functionals not explored in this work can be used.

Once the exchange-correlation functional is approached, a self-consistent field is ready to calculate χ of the interacting system through Eq. (3.42).

3.3. SOLVATION MODELS

In this section will be provided some ideas of how to model the solvation. Unlike previous sections the basic idea of this modelling will be explained. An exhaustive discussion of this topic can be consulted in ref 7 and 8.

Here it will be presented two methods, both are *polarizable continuum models*. PCM models do not represent the solvent explicitly but rather as a dielectric medium with surface tension at the solute-solvent boundary. This type modelling tries to avoid the unviable calculation of explicit solvent molecules around the solute. In the calculations of this work *SMD (solvent model density)* and *IEF-PCM (integral equation formalism-polarizable continuum model)* have been used.

The solvent is usually characterized by some or (as SMD) all of these parameters: The main parameter, the dielectric constant. Other parameters are refractive index, bulk surface tension and acidity and basicity parameters.

Once the solvent is parameterized a paramount issue is how is described the solvent-solute interaction, and this issue is mainly what makes the difference between different methods. Nevertheless, a common idea is to describe a cavity were the solute fits in. Out of this cavity, the continuum solvent. The cavity is performed through several criteria depending on the method, and do not must be "molecule shaped", as intuition may predict. For example, geometry and atomic numbers can be used to do so. However, the most physical definition of a solute cavity would surely depend on more details of the solute than just its geometry and the atomic numbers of its constituent atoms, and in fact some solvation models use cavities in which the radii depend on charges and/or atomic environments or the positions of isodensity contours. A precise definition of a solute cavity is uncertain, and actually the very concept of a solute cavity is an approximate one.

From a chemical reasoning, closest molecules of solvent experiments a stronger interaction with the solute (first solvation shell) and further shells are essentially bulk solvent. That means

that geometry of first solvation shell molecules will suffer a considerable change (also the geometry of the solute). Obviously, the solvent-solute interaction becomes stronger as long as the solvent becomes more polar. So, the continuum model must perform this consideration.

As the first solvation shell will always be the most important interaction, this methods focus on the solute-solvent boundary. This important issue is the most difficult to deal with, because as said before, solute cavity is an approximate concept, and several approximations and/or imprecise description of this interaction are granted.

Experimental parameters are used to fit some equations. These parameters are extracted from a set of well-chosen compounds, depending on which parameter is going to be fitted.

3.3.1. IEF-PCM model

Let us discuss some of the considerations taken into account in this method. As said a few lines before, this model approximate the solvent as a continuum medium, characterized by its dielectric constant ε, interacting with the solute molecule.

The solute can be performed in a quantum mechanical level or as a classical collection of point charges and is fitted in a cavity that host the solute, thus defining the solute-solvent interface as the cavity surface Γ. Mutual polarization of the solute and the continuum can be recast using boundary conditions. In fact, the cavity surface need to be discretized to carry out the required numerical surface integrations. Nevertheless this process leads to discontinuities, singularities and to an energy functional which is not smooth with respect to the parameters involved in its definition.

A big advantage of this methodology is that represents a very good compromise between accuracy, formal complexity, applicability and widespread availability.

3.3.2. SMD model

Essentially, SMD follows the philosophy of the PCM methods. The charge distribution of the solute (charge density) induces polarization in the surrounding dielectric medium, and the self-consistently determined interaction between the solute charge distribution and the electric polarization field of the solvent, when adjusted for the energetic cost of polarizing the solute and the solvent, constitutes what is called the electrostatic (or bulk electrostatic) contribution to the free energy of solvation. The electric potential of the solute, called the reaction field, equals to the total potential minus the electrostatic potential of the gas-phase solute molecule.

The total electric field satisfies the nonhomogeneous Poisson equation (NPE) for electrostatics. Therefore, the reaction field can be obtained self-consistently by numerical integration of the NPE coupled to the quantum mechanical electron density of the solute molecule.

Sadly, current methods based on the NPE have uncertainties due to the definition, size and shape of the solute cavity, the portion of the solute charge that may lie outside the cavity and the assumed way in which the permittivity changes at and near the solute-solvent boundary.

But what are the differences between using IEF-PCM or SMD model? SMD is a newer methodology and have some advantages respect of IEF-PCM. SMD parameters do not depend on charges or hybridization states, thus there are no discontinuities when the model is applied along reaction paths. Also adds a missing non-electrostatic term to the basic electrostatic picture. Furthermore, SMD is more versatile, because can be used in more free and commercial electronic structure packages and different chemical system yielding no more (nor less) accurate results as other PCM models.

3.4. DENSITY FUNCTIONAL DISPERSION CORRECTION

As for solvation modelling, this section will uniquely provide some considerations of a dispersion correction for DFT. Some methods, within them DFT, fail to describe with some accuracy the weak but physically and chemically very important London dispersion interactions. One could obviate these kind of interactions, but it would suppose a mistake, specially for non-polar molecules and solvents because, even weak, they can make the difference.

The dispersion correction used in this work was published by Stefan Grimme et al. (ref. 9). This method actually can be considered robust as it has been tested thoroughly and applied successfully now on thousands of different systems including inter- and intramolecular cases ranging from rare gas dimers to huge graphene sheets. Also has very nice properties of minor numerical complexity.

Grimme and co-workers achieved almost *ab initio* fashion consistent parameters for the entire set of chemically relevant elements with a minimal of empiricism. Nevertheless, the main drawback of this method is that is not dependent on and does not affect the electronic structure

in order to keep the numerical complexity low. This restriction ultimately limits the accuracy, in particular, for chemically unusual cases.

Moreover, other dispersion corrections are usually designed for a specific type of functional. Grimme's correction was designed as a correction for common functionals (as B3LYP, PBE or TPSS) that may be not optimal for non-covalent interactions but perform well for other important properties.

Compared to other corrections and previous versions, the current version (2010) has the following properties and advantages:

- Less empirical
- Asymptotically correct with all density functionals for finite systems (molecules) or non-metallic infinite systems (i.e. performs correctly the long-range interactions). It gives the almost exact dispersion energy for a gas of weakly interacting neutral atoms and smoothly interpolates to molecular regions.
- Good description of all chemically relevant elements (nuclear charge Z=1-94).
- Atom pair-specific dispersion coefficients and cutoff radii (interatomic distance region where the dispersion energy is decreasing) are explicit computed.
- New fractional coordination number (geometry) dependent dispersion coefficients are used that do not rely on atom connectivity information (differentiable energy expression).
- Similar of better accuracy for light molecules and a strongly improved description of metallic and heavier systems.

About empiricism, this method only requires adjustment of two global parameters for each density functional.

The overall of the dispersion correction gives a decrease of 15-40% in the mean absolute deviations compared to the previous version and spectacular improvements are found for a tripeptide-folding model and all tested metallic systems, were London interactions become paramount.

4. OBJECTIVES

This work is based on the work of Benedetta Mennucci and José M. Martínez (ref. 10). Their work was motivated as a first part of a study of solvation in peptides using quantum-mechanical and classical approaches. In this study, the peptide is modelled as its simple analogue, namely, the *N*-methylacetamide, and the effects of the solvent (water) are introduced at three different levels: continuum description, using solute-solvent clusters, and using the same clusters embedded in an external continuum. Finally, a UV and IR spectra are calculated and analyzed.

Here, the same topics are followed, although molecular dynamics discussion is entirely obviated. Quantum-mechanical topics are adapted, usually reduced to the most stable conformation or expanded in level of theory and solvation modelling in order of carry out the following objectives:

- Reproduce Mennucci and Martínez results.
- Discuss about differences in the geometry of *N*-methylacetamide in vacuum and in solvation (water) for different basis sets and solvation models.
- Introduce a dispersion correction and evaluate its role in calculations.
- Analyze UV and IR spectra in vacuum and in solvation.
- Study the solvation effects on geometry, UV and IR spectra and provide a simple justification.

5. COMPUTATIONAL DETAILS

Several calculations were performed to achieve the previous objectives. Here, it is presented how different inputs were elaborated in Gaussian 03 and Gaussian 09 (ref. 12 and 13).

5.1. SCANS AND GEOMETRY OPTIMIZATION

For all systems (single *trans*-NMA, *cis*-NMA and NMA clusters) both in vacuum and in solution, geometry optimizations were performed at the density functional theory using the

B3LYP hybrid functional. Two different basis set were used: 6-31+G(d,p) and 6-311++G(d,p). To the latter basis set Grimme's GD3BJ dispersion correction were added. IR spectra were computed in an optimization+IR calculation.

Scans of both methyl group were performed either in vacuum and in solution to probe which conformation is a true conformer and then, perform the geometry optimizations. This time, 6-31+G(d,p) basis set was used.

Also using 6-31+G(d,p) basis set, a scan of cis-trans conformations were executed in order to estimate the energetic barrier of this isomerisation.

For optimization and scan the convergence criteria is set to tight. Also, the grid used for DFT calculations is set ultrafine. Both criteria are needed in DFT to achieve good results.

5.2. SOLVATION

Two (actually, three) different solvation models were used for all systems. IEF-PCM solvation model were used in two different versions: Gaussian03 and Gaussian09. Although both versions uses the same modelling, they are slightly different. SMD solvation model were also used.

5.3. UV SPECTRA

To evaluate absorption energies, time-dependent DFT was used with B3LYP functional and the Dunning basis set with one diffuse (+) and one polarization (d) function on all O, N and C atoms (d95v+(d)). The same calculations were also performed for all system with a 6-311++G(d,p) basis set.

Calculations were performed with and without the Tamm-Dancoff approximation (TDA) to TD-DFT in order to test the quality of the approximation.

6. CONFORMATIONS AND CONFORMERS

N-methylacetamide has two possible isomers arise either in vacuum or in solution: *cis*-NMA and trans-NMA, each of them with several conformations. Experimental data show that both are not equally abundant but instead *trans*-NMA is dominant. The scan performed of cis-trans conversion yielded an energy barrier of ~20 kcal/mol. Following experimental and theoretical data, the cis-trans conversion is a high enough barrier to neglect *cis*-NMA conformations. Mennucci and Martínez reported four different conformations for *trans*-NMA.

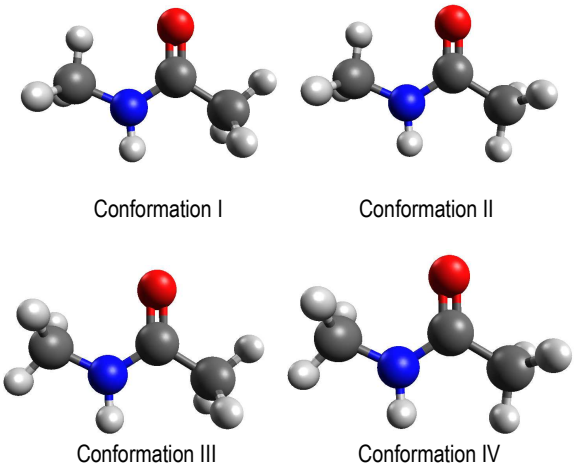

Figure 6.1. *Trans*-NMA conformations obtained by rotating methyl groups.

These four conformations (figure 6.1) were obtained through performance of scan rotation of both methyl groups. When one methyl is being rotated, the other is kept fixed. The scan plots can be shown in appendix 2.

The relative stabilities of the four conformers largely depends on the solvation, although conformation II is the most stable in the gas phase, structure IV becomes the most stable in water. The vibrational analysis of the four structures reveals that these are the only real minima (all eigenvalues of the force constant matrix are positive). The other two structures present two imaginary frequencies corresponding to a methyl rotations. These rotations lead to the most stable conformation either in vacuum or solvation as expected.

Mennucci and Martínez (ref. 10) point that when changing the B3LYP functional to MP2 in the calculations of the conformations and an increasing on the basis set to 6-311++G(d,p),

structure IV becomes the lowest stationary conformation and structure II is the second most stable structure in vacuum, but with a negative frequency. This behaviour is not reproduced in calculations presented in this work and structure II keeps being the most stable structure in vacuum. Nevertheless, energetic barriers of the scans of methyl groups agrees with experimental and theoretical conclusions: although only one conformation is a true conformer, methyl rotations in vacuum and in solvation are almost free rotations.

For hydrated NMA, any level of calculations indicates conformer IV as the minimum energy one, a fact confirmed by previous calculations and by crystallographic data. The calculations performed agree with this assumption. Table 6.1 compares optimized geometries calculated in this work with Mennucci and Martínez calculations and experimental data (ref. 10).

	II vacuum[a]	IV water[b]	Mennucci Martínez, II vacuum	Mennucci Martínez, IV water	Electron diffraction	Crystal
CO	1.221	1.247	1.229	1.243	1.225	1.236
CN	1.366	1.342	1.368	1.351	1.386	1.290
NH	1.007	1.009	1.009	1.010	(1.002)	-
$NC_{m'}$	1.453	1.456	1.454	1.458	1.469	1.465
CC_m	1.518	1.506	1.520	1.515	1.520	1.536
C_mCN	115.3	116.9	115.6	116.9	114.1	116.5
OCN	122.9	121.7	122.8	121.7	121.8	123.0
CNH	118.4	118.5	118.4	118.9	110.0	119.0
$CNC_{m'}$	122.8	122.7	123.0	122.4	119.7	120.5
$\psi(HC_mCN)$	-0.018	5.5	0.4	1.3	-	0
$\varphi(CNC_{m'}H)$	-0.911	-178.2	0.4	179.5	-	180.0
OCNH	178.8	179.3	180.0	180.0	180.0	180.0
$C_mCNC_{m'}$	-179.9	179.8	180.0	180.0	180.0	180.0

a) B3LYP/6-311++G(d,p) + Grimme's correction.

b) B3LYP/6-311++G(d,p) + SMD + Grimme's correction.

Mennucci and Martínez results: B3LYP/6-31+G(d,p) and IEF-PCM for water modelling.

Bond length are in angstroms and angles are in degrees. Indices m and m' distinguish methyl carbon to CO and methyl carbon to NH.

Table 6.1. Comparison optimized geometries in this work and calculated and experimental data (ref. 10).

Crystallographic experimental data in table 6.1 stands for conformer IV. Experimental data for conformer II in vacuum were obtained via electron diffraction. Although little fluctuations can be seen, the overall of the experimental and calculated data agrees in a very good degree. As expected, NMA keeps planar symmetry in order to maintain conjugation between O=C-N atoms.

As already indicated, φ(CNC_mH) dihedral angle passes from ~0º to ~180º in solution. This can be related to the more favourable intramolecular interaction between the lone pair electrons of the oxygen and the eclipsed hydrogen of the methyl group in the isolated NMA, this interaction being reduced in solution by interactions with the solvent. Also an increase on the C=O bond length passing from gas to water is observed. This behaviour is expected for solvents with strong solute-solution interactions. Hence, a red-shifted stretching frequency is expected. A decrease of the CN bond length is observed as an increase of double bond character between CN atoms in consequence of the C=O elongation. A further discussion of this issue will be provided in section 7.

A full table of the geometries obtained from the calculations proposed in section 5.1 can be seen in appendix 1.

7. H-BONDING EFFECTS: NMA-CLUSTER

In the previous section differences between vacuum and water geometries have been discussed. Nevertheless, water interacts strongly with its solute. Hydrogen bonds are expected in NMA. Specifically O···HOH and H···OH_2 hydrogen bonds are expected.

Mennucci and Martínez performed five different clusters to take into account this interactions difficult to handle for continuum modelling of solvation. In this section, only the best cluster either in water and vacuum is considered (figure 7.1). A further discussion of the different clusters can be shown in Mennucci and Martínez work, section 5.

In table 7.1, a comparison between calculations from this work and from ref. 10 is shown. All data are in a very tight agreement. When clusters are calculated, either in vacuum or in solvation conformer IV becomes the unique true conformer.

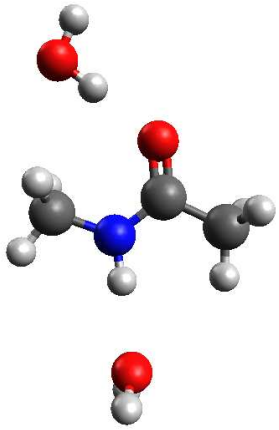

Figure 7.1. NMA-cluster considered in this work.

	vacuum cluster[a]	water cluster[b]	Mennucci Martínez vacuum cluster	Mennucci Martínez water cluster
CO	1.233	1.253	1.240	1.252
CN	1.349	1.335	1.352	1.342
NH	1.012	1.019	1.014	1.020
$NC_{m'}$	1.457	1.457	1.459	1.458
CC_m	1.515	1.505	1.518	1.513
C_mCN	116.2	117.1	-	-
OCN	122.9	122.4	-	-
CNH	119.0	119.0	-	-
$CNC_{m'}$	122.0	122.6	-	-
ψ(HC_mCN)	0.0	1.1	0.1	0.2
φ($CNC_{m'}H$)	180.0	175.7	179.9	179.9
OCNH	180.0	-0.044	-	-
$C_mCNC_{m'}$	180	0.024	-	-

a) B3LYP/6-311++G(d,p) + Grimme's correction.

b) B3LYP/6-311++G(d,p) + SMD + Grimme's correction.

Mennucci and Martínez results: B3LYP/6-31+G(d,p) and IEF-PCM for water modelling (ref. 10).

Bond length are in angstroms and angles are in degrees. Indices m and m' distinguish methyl carbon to CO and methyl carbon to NH.

Table 7.1. Comparison of best calculated geometries in this work and calculated data.

When H-bonding is modelled by explicitly including water molecules it is expected that CO bond length increase even more than the increasing obtained for the continuum model. This can be understood readily: atomic bonding between atoms with a big electronegativity difference is, in a simple way, an essentially electrostatic interaction. Thus, an atom with a positive partial charge (H) interacts with the partially negative charged atom (O), the C=O will be stretched. In consequence, CN bond is shorten.

For the isolated NMA-cluster, this behaviour is also observed, although not that strongly as for the NMA-cluster in solution. This fact suggest that solute-solvent interactions in other parts of the molecule are also important in this behaviour, because the amide group induces positive partial charges to the whole molecule, increasing the non-polar groups interaction with the solvent. Figure 7.2 illustrates this issue.

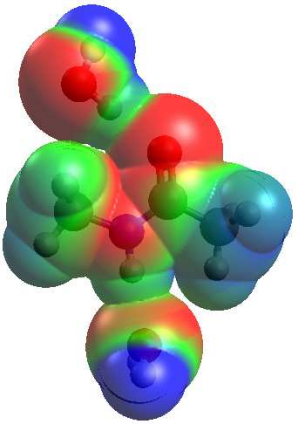

Figure 7.2. Electrostatic potential of NMA-cluster. Cool colours represent positive charged zones. Warm colours represent negative charged zones.

8. IR SPECTRA

Here we shall focus on the changes in the frequencies of four fundamental bands: Amide I, amide II, amide III and amide NH bands when passing from vacuum to solvation. Knowing changes in previous geometries, it should be possible to understand the shifts in these four fundamental bands.

Due to the neglect of anharmonicity effects and to the approximate treatment of electron correlation, vibrational frequencies are typically larger than those observed experimentally. In order to correct these deviations, optimum frequency scale factors have been determined for many QM levels of theory. The different scale factors can be consulted in ref. 11. Sadly, do not exist a scale factor for the basis set used in this work. Mennucci and Martínez computed their own scale factor.

Amide I (AI) generally appears as the most intense band in the IR spectra of peptides and proteins. It is usually described as a pure C=O stretching, even if the normal-mode pattern is more complex, as in this case. Tables 6.3 and 6.4 shows the calculated spectra for vacuum and solution respectively in comparison with Mennucci and Martínez and experimental data. Computational calculations fits well with experimental records, although some considerations must be discussed.

Vacuum IR [cm-1]	**AI**	**AII**	**AIII**	**N-H**
Conformer II[a]	1751	1523	1345	3617
Mennucci Martínez conformer II	1750	1551	1284	3668
Experimental[b]	1723	1500	1265	3476/3460

a) B3LYP/6-311++G(d,p) + Grimme's correction. + SMD when solvation.

b) From ref. 10.

Mennucci and Martínez results: B3LYP/6-31+G(d,p) (ref. 10).

Table 8.1. Vacuum fundamental bands of NMA IR spectrum.

AI band is red-shifted passing from vacuum to water in all cases. This behaviour is totally expected since C=O bond length is increased in water in comparison to vacuum. Mennucci and

Martinez in a further discussion of this band, determined that C=O stretching in less affected by rotational effects since is almost identical in all conformations. Also, in their discussion they conclude, via their vacuum and water cluster IR calculated data, that the cluster model yields an improved value for the frequency of this band. This suggest that not only solvent interactions of the C=O group are important for this band, other parts of de molecule being also affected. This assumption agrees with calculations performed in this work, however, Mennucci and Martínez obtain an underestimated red-shift. Contrary, this work calculations yields an overestimated red-shift for this band. Since the calculations made add a dispersion correction and a larger basis set, better accuracy should be expected. The overestimation on the red-shift can be understood if it is considered that, in fact, the H-bonded water molecule is not fixed in the cluster and is exchanged with other water molecules. Hence, a lower average hydrogen-bond interaction and a higher wavenumber are expected.

It must be noticed that geometries of water NMA and water cluster differ markedly. Hence, a notable difference on frequencies should be expected. However, when cluster vibrations are analyzed, AI band includes vibrations of hydrogen-bonded water molecules. This new vibrations in respect of the continuum solvated NMA countervail, somehow, the geometric differences.

Water IR [cm-1]	**AI**	**AII**	**AIII**	**N-H**
IV water[a]	1606	1557	1300	3622
IV vaccuum Cluster[a]	1711	1589	1317	3563
IV water Cluster[a]	1601	1588	1332	3423
Mennucci Martínez Vacuum cluster	1718	1591	1322	3572
Mennucci Martínez Water cluster	1651	1609	1340	3454
Experimental[b]	1625	1582/1575	1316	3314

a) B3LYP/6-311++G(d,p) + Grimme's correction. + SMD when solvation.

b) From ref. 10

Mennucci and Martínez results: B3LYP/6-31+G(d,p) (ref. 10).

Table 8.2. Water fundamental bands of NMA IR spectrum.

As a final note, expected splitting of the AI band due to the mixing with H_2O bending vibration of the hydrogen-bonded water is present in theoretical calculations.

Amide II (AII) is described as an out-of-phase combination of CN stretching and CNH bending. Obviating CNH bending, a blue-shifted frequency is expected when NMA spectrum is performed in solvation given that CN bond is shorter in water. As predicted, computational calculations predict a blue-shift of this frequency. As AI vibration, AII band is specially sensitive to H-bond interaction since when continuum solvation model is added to vacuum cluster, this band remains at the same frequency. When explicit water molecules are considered, a greater blue-shift than only continuum solvation calculation is obtained and the performance of AII band is highly improved, very close to the experimental value.

This band is not overestimated because dominant vibration (CN stretching) is indirectly influenced of hydrogen bond and many other interactions counteract the overestimation, mainly the N-H···HOH bond.

Amide III (AIII) band is the counterpart to amide II, being primarily CNH bending plus CN stretching, exactly the *vice versa* vibration. This is by far the most difficult band to understand, because geometry does not provide a clear answer. Focusing on the shift passing from vacuum to solvation, it is clear that a blue-shift is expected. Theory reproduces this shift as well.

An unexpected result has been obtained for this frequency: vacuum cluster gives exactly the experimental value. When calculations were proposed, it was supposed that water cluster NMA would always produce the best results. Nonetheless, a possible explanation will be also provided for this result: Hydrogen bond is a directional interaction (i.e. stronger for an specified direction), thus, if a vibration implies a change in this direction, a blue-shifted frequency is expected. So, AIII is mainly a CNH bending. Hence, when a directional interaction (the explicit H-bond) is considered, the bending frequency is blue shifted. Vacuum cluster provides an exact value, whereas water cluster overestimates this effect, as shown for AI. This overestimation can also seen in Mennucci and Martínez results.

Finally, N-H band describes a pure N-H bond stretching. This is, by far, the worse performed band. By reasons explained above, it is expected an experimental and theoretical red-shift of this band when solvated in water. But, the shift is notably underestimate even in water cluster calculations. N-H is a tricky band since the proton implied in the bonding is slightly exchangeable with water. Thus, the mean experimental bond length is larger than the

theoretical one, where proton exchange is not considered. This argument is supported by the highly temperature sensitivity of the position and shape of the band. Also, it should be considered in further calculations the formation of a dimer where a possible C=O···H-N interaction is taken into account.

It all together suggests that a compromise between explicit water molecules and continuum solvation model should improve the accuracy of the prediction of IR spectra, specially for those bands strongly influenced by hydrogen bonding. It is also seen that not only interactions but exchanging of water molecules is important to improve the accuracy.

9. UV SPECTRA

The electronic absorption spectrum of NMA presents two different bands. These bands have been assigned to transitions $n \rightarrow \pi^*$ and $\pi \rightarrow \pi^*$. Figure 9.1 shows the orbitals implied in these transitions.

Mennucci and Martínez indicate in their discussion (ref. 10) that $n \rightarrow \pi^*$ implies a transition from HOMO to LUMO+x orbitals. The transition for $\pi \rightarrow \pi^*$ is from HOMO-1 to LUMO+x. They also give a value of x=1 when NMA is solvated and x=2 in vacuum. The analysis of calculations shown in table 9.1 and 9.2, however, does not agree with this assumption. Depending on the level of theory and the solvation model used, HOMO and HOMO-1 can exchange its positions and x can take values from 1 to 4. This analysis could seem totally unexpected, but since the orbitals implied in this transitions are almost degenerated, different levels of theory or solvation can change readily its relative positions. Accordingly, these transitions have contributions from two or three Slater determinants differing in one orbital. Nevertheless, the main contribution is kept as a $n \rightarrow \pi^*$ or $\pi \rightarrow \pi^*$ transition.

For both tables TD-DFT theory were used. Nevertheless, TDA yielded very similar results. Both tables are in very good agreement with Mennucci and Martínez results and experimental data. However, some issues can be discussed, although calculations for this system are not very sensitive to solvation or a change in the basis set.

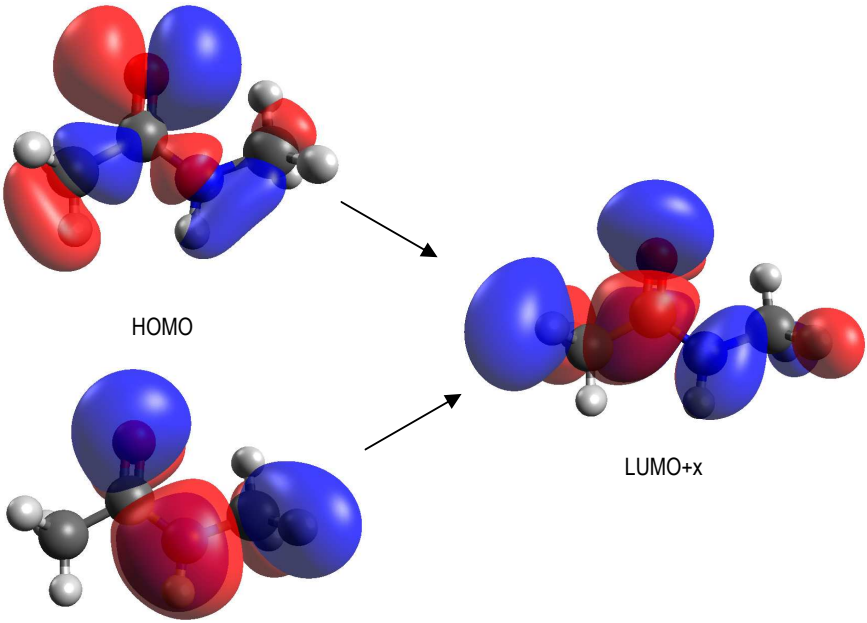

Figure 9.1. Plot of the orbitals involved in the two transitions. x can adopt different values.

UV [eV]	**n → π***	**π → π***
II vaccuum 6-31+G(d.p)	5.7 (218)	7.1 (175)
II vaccuum 6-311++G(d.p)	5.7 (218)	7.1 (175)
Mennucci Martínez vacuum II	5.7 (218)	7.1 (175)
Experimental	5.5 (226)[a]	6.8 (182)

a) in ciclohexane
In parenthesis, the wavelength expressed in nm.
Mennucci and Martínez results: B3LYP/6-31+G(d,p) (ref. 10).
Experimental data from ref. 10.

Table 9.1. Absorption spectra for isolated NMA.

UV [eV]	**n → π***	**π → π***
Water IV 6-31+G(d,p) IEF-PCM	5.8 (214)	7.0 (177)
Water IV 6-31+G(d,p) SMD	5.9 (210)	7.0 (177)
Water IV 6-311++G(d,p) IEF-PCM	5.8 (214)	7.0 (177)
Water IV 6-311++G(d,p) SMD	6.0 (207)	7.0 (177)
Mennuci and Martínez Water IV	5.8 (214)	7.0 (177)
Experimental	5.7 (218)	6.7 (185)

In parenthesis, the wavelength expressed in nm.
Mennucci and Martínez results: B3LYP/6-31+G(d,p) (ref. 10).
Experimental data from ref. 10.

Table 9.2. Absorption spectra for water NMA.

Experimental data present a blue shift in n → π* transition. This shift is expected since the promotion of the electron reduces the permanent dipole of C=O bond and thus, the excited state is less strongly stabilized in polar solvents with respect to the ground state. Calculations reproduce well the sign of this shift. All type of calculations leads to almost the same results, but SMD solvation model overestimates somewhat this blue shift.

For π → π* transition, a slight red-shift is observed experimentally. This shift is also well reproduced in the calculations. This shift is so low that they may lay within the computational accuracy. However, all different calculations agree perfectly with each other either in vacuum or solvation. A red-shifted frequency is expected because the C=O bond length is longer in solution, hence, π orbital suffers an increase on its energy. All levels of theory and solvation reproduce the same value possibly because a purely geometrical change is responsible of the shift, and then the different errors or improvements introduced by the level of theory of solvation are fully counteracted.

A general issue for both transition and either in vacuum or solvation is that calculated values are systematically greater than the experimental about 0.1 and 0.3 eV. This can be a consequence of having computed vertical transitions (section 3.2.3). Hence, the relaxation the excited state is not taken into account. This yields an overestimation of the excitation energy. Another source of error is that TD-DFT only includes monoexcited determinants, while a good description of electronic excited states may require including Slater determinants differing in more than one orbital from the ground state one.

Apart of technical issues, also experimental errors must be taken into account: Due to its vibrational structure, UV bands are very wide, hence, an inherent error in the determination of the position of the band must be considered.

10. CONCLUSIONS

Along the document several issues about the effects of solvation on *N*-methylacetamide IR and UV spectra have been discussed. From experimental data and theoretical calculations some general ideas can be extracted that can be used for other systems:

The difference between the geometry of isolated and solvated molecules can be used to predict the shift of a their vibrational frequencies, specially for stretching modes. If the bond involved in the stretching mode is elongated when solvated, the bonding is weaker, and then a red-shifted frequency is expected. Explicit water molecules improves the description of hydrogen-bonds as compared to the continuous solvent models, and a dispersion correction to DFT results leads to a better performance for this type of bonding. Nevertheless, the use of a continuous solvent model together with explicit water molecules usually overestimates this interaction.

Bending or complex vibrations frequencies shifts can be also predicted, although a more accurate explanation must be provided. Also, special attention must be paid to N-H stretching band where an exchangeable proton is involved. These frequency is generally underestimated even when an NMA solvated cluster is performed.

UV spectra appear to be less sensitive to solvation than IR spectra. IR vibrations present strong deviations passing from vacuum to solvation. Nevertheless, red or blue shifts can be also predicted. $n \rightarrow \pi^*$ transition is blue-shifted from vacuum to solvation because lone pairs are stabilized when they interact with water. SMD solvation model either for NMA or NMA cluster overestimates blue shift. $\pi \rightarrow \pi^*$ is red-shifted when the double bond interacts strongly with the solvent. The elongation of the double bond produces an increment of the π orbital energy, and hence, a decrease of the excitation energy. The deviations of the calculated frequencies with respect to the experimental ones are probably due to the lack of excited state geometry relaxation and to an incomplete description of its electronic structure.

11. REFERENCES AND NOTES

1. Paniagua, J.C.; Alemany, Pere. *Química quàntica: vol.II,* 1a ed.; Llibres de l'Índex, 2000.
2. Paniagua, J.C.; Alemany, Pere. *Química quàntica: vol.III,* 1a ed.; Llibres de l'Índex, 2000.
3. Cramer, Christopher J. *Essentials of computational chemistry: Theories and models,* 2nd ed.; Wiley, 2004.
4. Paniagua, J.C. *Métodos basados en funcionales de la densidad*, 2006.
5. Marques, M.A.L.; Gross, E.K.U. Time-Dependent Density Functional Theory. *Annu. Rev. Phys. Chem.* **2004**, 55, 427-455.
6. Casida, M.E.; Huix-Rotllant, M. Progress in Time-Dependent Density-Functional Theory. *Annu. Rev. Phys. Chem.* **2012**, 63, 287-323.
7. Scalmani, G.; Frisch, M.J. Continuous surface charge polarizable continuum models of solvation. I. General formalism. *J. Chem. Phys.* **2010**, 132, 114110.
8. Marenich, A.V.; Cramer, C.J.; Truhlar, D.G. Universal Solvation Model Based on Solute Electron Density and on a Continuum Model of the Solvent Defined by the Bulk Dielectric Constant and Atomic Surface Tensions. *J. Phys. Chem.* **2009**, 113, 6378-96.
9. Grimme, S.; Antony, J.; Ehrlich, S.; Krieg, H. A consistent and accurate ab initio parameterization of density functional dispersion correction (DFT-D) for the 94 elements H-Pu. *J. Chem. Phys.* **2010**, 132, 154104.
10. Mennucci, B.; Martínez, J. M. How to Model Solvation of Peptides? Insights from a Quantum-mechanical and Molecular Dynamics Study of *N*-Methylacetamide. 1. Geometries, Infrared, and Ultraviolet Spectra in Water. *J. Phys. Chem.* **2005**, 109, 9818-9829.
11. Precomputed vibrational scaling factors. http://cccbdb.nist.gov/vibscalejust.asp
12. Gaussian 03, Revision D.02, Frisch, M. J.; Trucks, G. W.; Schlegel, H. B.; Scuseria, G. E.; Robb, M. A.; Cheeseman, J. R.; Montgomery, Jr., J. A.; Vreven, T.; Kudin, K. N.; Burant, J. C.; Millam, J. M.; Iyengar, S. S.; Tomasi, J.; Barone, V.; Mennucci, B.; Cossi, M.; Scalmani, G.; Rega, N.; Petersson, G. A.; Nakatsuji, H.; Hada, M.; Ehara, M.; Toyota, K.; Fukuda, R.; Hasegawa, J.; Ishida, M.; Nakajima, T.; Honda, Y.; Kitao, O.; Nakai, H.; Klene, M.; Li, X.; Knox, J. E.; Hratchian, H. P.; Cross, J. B.; Bakken, V.; Adamo, C.; Jaramillo, J.; Gomperts, R.; Stratmann, R. E.; Yazyev, O.; Austin, A. J.; Cammi, R.; Pomelli, C.; Ochterski, J. W.; Ayala, P. Y.; Morokuma, K.; Voth, G. A.; Salvador, P.; Dannenberg, J. J.; Zakrzewski, V. G.; Dapprich, S.; Daniels, A. D.; Strain, M. C.; Farkas, O.; Malick, D. K.; Rabuck, A. D.; Raghavachari, K.; Foresman, J. B.; Ortiz, J. V.; Cui, Q.; Baboul, A. G.; Clifford, S.; Cioslowski, J.; Stefanov, B. B.; Liu, G.; Liashenko, A.; Piskorz, P.; Komaromi, I.; Martin, R. L.; Fox, D. J.; Keith, T.; Al-Laham, M. A.; Peng, C. Y.; Nanayakkara, A.; Challacombe, M.; Gill, P. M. W.; Johnson, B.; Chen, W.; Wong, M. W.; Gonzalez, C.; and Pople, J. A.; Gaussian, Inc., Wallingford CT, **2004**.
13. Gaussian 09, Revision D.01, Frisch, M. J.; Trucks, G. W.; Schlegel, H. B.; Scuseria, G. E.; Robb, M. A.; Cheeseman, J. R.; Scalmani, G.; Barone, V.; Mennucci, B.; Petersson, G. A.; Nakatsuji, H.; Caricato, M.; Li, X.; Hratchian, H. P.; Izmaylov, A. F.; Bloino, J.; Zheng, G.; Sonnenberg, J. L.; Hada, M.; Ehara, M.; Toyota, K.; Fukuda, R.; Hasegawa, J.; Ishida, M.; Nakajima, T.; Honda, Y.; Kitao, O.; Nakai, H.; Vreven, T.; Montgomery, J. A., Jr.; Peralta, J. E.; Ogliaro, F.; Bearpark, M.; Heyd, J. J.; Brothers, E.; Kudin, K. N.; Staroverov, V. N.; Kobayashi, R.; Normand, J.; Raghavachari, K.; Rendell, A.; Burant, J. C.; Iyengar, S. S.; Tomasi, J.; Cossi, M.; Rega, N.; Millam, N. J.; Klene, M.; Knox, J. E.; Cross, J. B.; Bakken, V.; Adamo, C.; Jaramillo, J.; Gomperts, R.; Stratmann, R. E.; Yazyev, O.; Austin, A. J.; Cammi, R.; Pomelli, C.; Ochterski, J. W.; Martin, R. L.; Morokuma, K.; Zakrzewski, V. G.; Voth,

G. A.; Salvador, P.; Dannenberg, J. J.; Dapprich, S.; Daniels, A. D.; Farkas, Ö.; Foresman, J. B.; Ortiz, J. V.; Cioslowski, J.; Fox, D. J. Gaussian, Inc., Wallingford CT, **2009**.

12. ACRONYMS

B3LYP: Becke, three-parameter, Lee-Yang-Parr exchange-correlation functional

DFT: Density Functional Theory

GGA: Generalized Gradient Approximation

GTO: Gaussian Type Orbital

HK(H-K): Hohenberg-Kohn

HOMO: Highest Occupied Molecular Orbital

IEF-PCM: Integral Equation Formalism-Polarizable Continuum Model

IR: InfraRed

KS(K-S): Kohn-Sham

LDA: Local Density Approximation

LSDA: Local Spin Density Approximation

LUMO: Lowest Unoccupied Molecular Orbital

m-GGA: meta-Generalized Gradient Approximation

MPn: n-order Møllet-Plesset perturbation theory

NMA: *N*-MethylAcetamide

NPE: Nonhomogeneous Poisson Equation

SCF: Self-Consisted Field

SMD: Solvation Model Density

STO: Slater Type Orbitals

TDA: Tamm-Dancoff Approximation

TD-DFT: Time-Dependent Density Functional Theory

UV: UltraViolet

XC: eXchange-Correlation

APPENDICES

APPENDIX 1: GEOMETRY TABLES

DFT B3LYP 6-31+G(d.p)	IV water iefpcm g03	IV water iefpcm g09	IV water smd g09	IV water cluster iefpcm g03	IV water cluster iefpcm g09	IV water cluster smd g09	IV cis water iefpcm g03	IV cis water iefpcm g09	IV cis water smd g09
CO	1.24525	1.24256	1.25406	1.25195	1.25125	1.25968	1.24666	1.24367	1.25556
CN	1.34941	1.35219	1.34436	1.34187	1.34246	1.33808	1.35175	1.35522	1.34708
NH	1.02169	1.00943	1.01128	1.02221	1.01936	1.02079	1.02506	1.01203	1.01355
NC_m	1.45761	1.45739	1.45852	1.45710	1.45741	1.45864	1.46030	1.46039	1.46130
CC_m	1.51588	1.51602	1.50862	1.51405	1.51359	1.50733	1.51543	1.51496	1.50764
C_mCN	116.802	116.606	117.081	116.755	116.901	117.442	117.120	116.986	117.485
OCN	121.907	121.854	121.654	122.628	122.609	122.265	121.270	121.089	120.820
CNH	119.511	118.849	118.398	119.201	119.172	119.112	115.537	115.110	115.890
CNC_m	122.246	122.657	122.881	122.555	122.635	122.681	126.229	126.769	126.041
ψ(HC_mCN)	0.050	-0.662	-1.126	-0.365	0.074	0.935	-179.987	-179.911	-179.480
φ(CNC_mH)	179.702	-178.015	-179.315	179.750	-179.970	176.729	-179.919	-179.888	-177.100
OCNH	179.785	179.431	-179.858	179.919	179.986	179.180	-0.029	-0.030	-0.773
C_mCNC_m	-179.939	-179.835	-179.944	-179.906	-179.986	-178.635	-0.030	0.047	1.094
Total energy	-248.56487	-248.56045	-248.56508	-401.46811	-401.45839	-401.46928	-248.56190	-248.55697	-248.56143

DFT B3LYP 6-311++G(d.p)	IV water iefpcm g03	IV water iefpcm g09	IV water smd g09	IV water cluster iefpcm g03	IV water cluster iefpcm g09	IV water cluster smd g09	IV cis water iefpcm g03	IV cis water iefpcm g09	IV cis water smd g09
CO	1.23814	1.23519	1.24676	1.24515	1.24468	1.25333	1.23961	1.23616	1.24823
CN	1.34085	1.35001	1.34186	1.34040	1.33935	1.33451	1.35060	1.35333	1.34492
NH	1.01992	1.00738	1.00918	1.02005	1.01770	1.01941	1.02348	1.01015	1.01159
NC_m	1.45771	1.45573	1.45636	1.45666	1.45537	1.45652	1.45971	1.45857	1.45955
CC_m	1.51454	1.51332	1.50576	1.51274	1.51068	1.50450	1.51416	1.51247	1.50505
C_mCN	116.611	116.337	116.888	116.564	116.563	117.138	116.921	116.465	117.051
OCN	122.041	121.969	121.749	122.714	122.705	122.409	121.400	121.398	121.079
CNH	119.525	118.619	118.545	119.131	118.958	119.046	115.557	115.404	116.091
CNC_m	122.243	122.433	122.664	122.537	122.508	122.598	126.315	126.396	125.756
ψ(HC_mCN)	0.116	-0.805	5.535	-0.521	-0.232	1.079	179.872	179.087	-179.703
φ(CNC_mH)	-179.889	-178.179	-178.172	179.848	179.962	175.728	179.929	177.936	-177.709
OCNH	179.829	179.472	179.255	179.954	180	179.064	-0.044	0.527	-0.732
C_mCNC_m	-179.952	-179.817	179.803	-179.947	-179.973	-178.600	0.024	-0.838	1.078
Total energy	-248.62181	-248.63044	-248.63488	-401.57294	-401.58208	-401.59271	-248.61858	-248.62733	-248.63166

DFT B3LYP 6-31+G(d.p)	II Vacuum	Vacuum Cluster	vacuum CIS
CO	1.22859	1.23982	1.22897
CN	1.36839	1.35171	1.37022
NH	1.00871	1.01395	1.01144
$NC_{m'}$	1.45446	1.14863	1.45513
CC_m	1.52021	1.51754	1.51945
C_mCN	115.646	116.500	116.675
OCN	122.800	122.762	121.050
CNH	118.406	119.254	113.807
$CNC_{m'}$	122.982	122.057	127.074
$\psi(HC_mCN)$	-0.007	0.006	-177.713
$\varphi(CNC_{m'}H)$	-0.464	179.991	-170.653
OCNH	179.926	-179.996	-3.334
$C_mCNC_{m'}$	-179.966	180	5.644
Total energy	-248.54875	-401.43834	-248.54499

DFT B3LYP 6-311G(d.p)	II Vacuum	Vacuum Cluster	vacuum CIS
CO	1.22100	1.23298	1.22118
CN	1.36649	1.34894	1.36862
NH	1.00669	1.01193	1.00947
$NC_{m'}$	1.45306	1.45684	1.45357
CC_m	1.51771	1.51481	1.51710
C_mCN	115.338	116.161	116.153
OCN	122.904	122.885	121.357
CNH	118.427	119.011	114.097
$CNC_{m'}$	122.795	121.983	126.733
$\psi(HC_mCN)$	-0.018	0.008	178.110
$\varphi(CNC_{m'}H)$	-0.911	179.991	172.102
OCNH	178.848	180	3.292
$C_mCNC_{m'}$	-179.926	-179.995	-5.630
Total energy	-248.61905	-401.56279	-248.61561

Bond length are in angstroms and angles are in degrees. Indices m and m' distinguish methyl carbon to CO and methyl carbon to NH. Total energy is in Hartrees.

APPENDIX 2: SCAN PLOTS

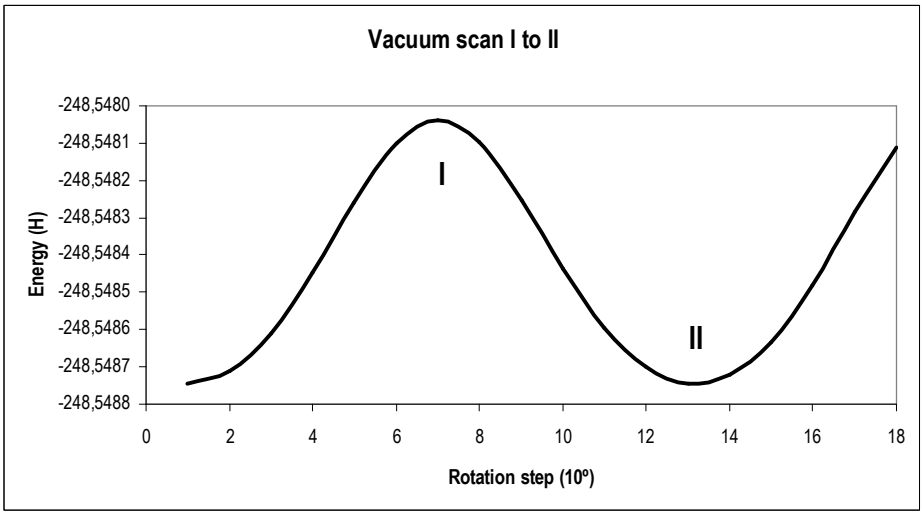

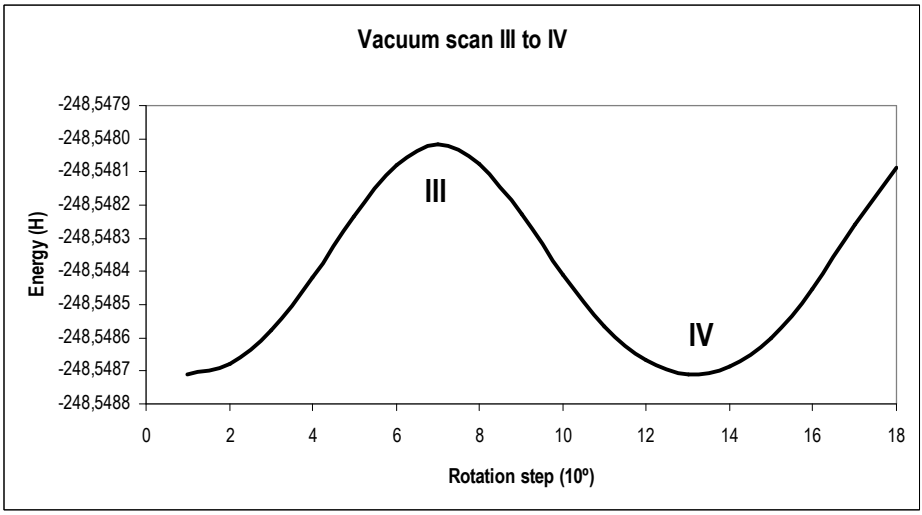

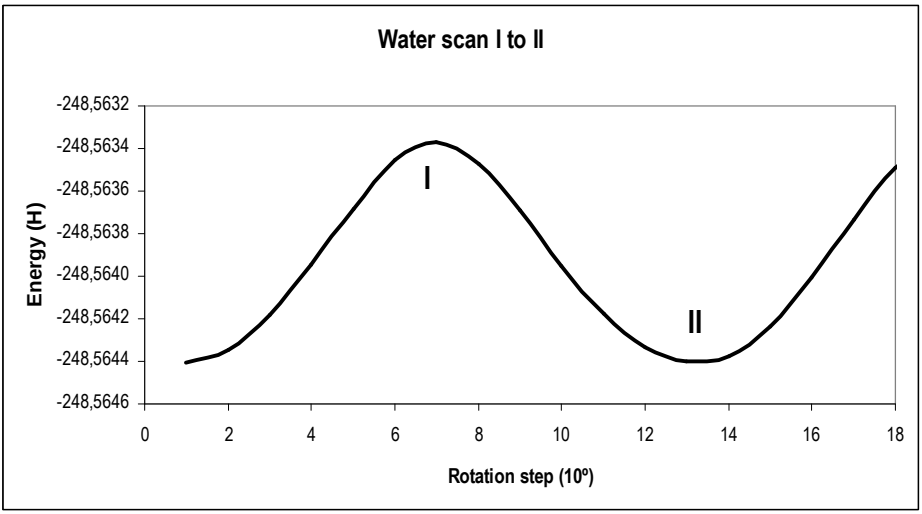

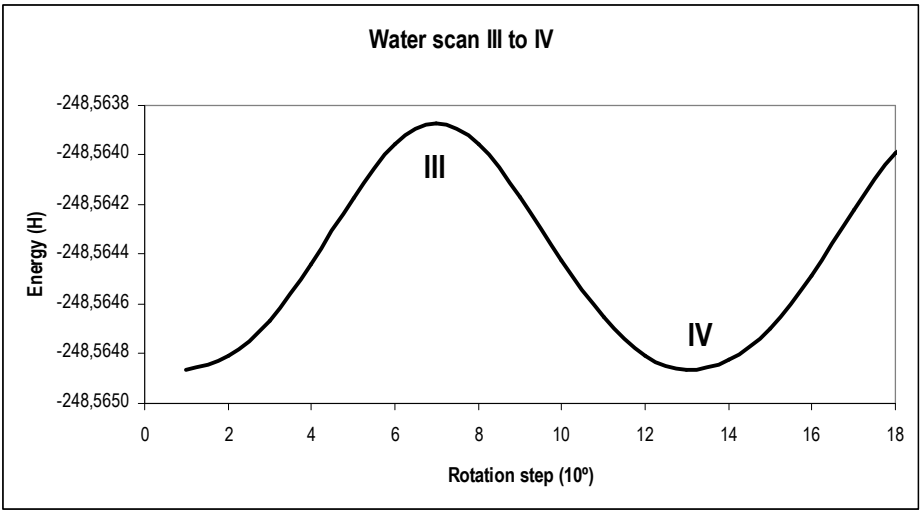

The previous plots show the rotation of the C_m methyl group for scan from structure I to structure II. For structure III to structure IV scan, $C_{m'}$ methyl group is rotated. When C_m or $C_{m'}$ methyl group is being rotated, the other is kept fixed.